JACS
JOURNAL OF THE AMERICAN CHEMICAL SOCIETY
Article
pubs.acs.org/JACS

Carbon Nitride–Aromatic Diimide–Graphene Nanohybrids: Metal-Free Photocatalysts for Solar-to-Hydrogen Peroxide Energy Conversion with 0.2% Efficiency

Yusuke Kofuji,[†] Yuki Isobe,[†] Yasuhiro Shiraishi,*[,†,§] Hirokatsu Sakamoto,[†] Shunsuke Tanaka,[∥] Satoshi Ichikawa,[‡] and Takayuki Hirai[†]

[†]Research Center for Solar Energy Chemistry, and Division of Chemical Engineering, Graduate School of Engineering Science and [‡]Institute for NanoScience Design, Osaka University, Toyonaka 560-8531, Japan

[§]Precursory Research for Embryonic Science and Technology (PRESTO), Japan Science and Technology Agency (JST), Saitama 332-0012, Japan

[∥]Department of Chemical, Energy and Environmental Engineering, Kansai University, Suita 564-8680, Japan

Supporting Information

ABSTRACT: Solar-to-chemical energy conversion is a challenging subject for renewable energy storage. In the past 40 years, overall water splitting into H_2 and O_2 by semiconductor photocatalysis has been studied extensively; however, they need noble metals and extreme care to avoid explosion of the mixed gases. Here we report that generating hydrogen peroxide (H_2O_2) from water and O_2 by organic semiconductor photocatalysts could provide a new basis for clean energy storage without metal and explosion risk. We found that carbon nitride–aromatic diimide–graphene nanohybrids prepared by simple hydrothermal–calcination procedure produce H_2O_2 from pure water and O_2 under visible light ($\lambda > 420$ nm). Photoexcitation of the semiconducting carbon nitride–aromatic diimide moiety transfers their conduction band electrons to graphene and enhances charge separation. The valence band holes on the semiconducting moiety oxidize water, while the electrons on the graphene moiety promote selective two-electron reduction of O_2. This metal-free system produces H_2O_2 with solar-to-chemical energy conversion efficiency 0.20%, comparable to the highest levels achieved by powdered water-splitting photocatalysts.

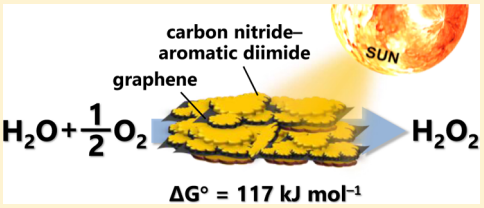

INTRODUCTION

Artificial photosynthesis, a photochemical reaction to convert sustainable resources into fuels by sunlight, is one of the most urgent and challenging issues.[1,2] Overall water splitting by semiconductor-based photocatalysts or photoelectrochemical cells into stoichiometric amounts of H_2 and O_2 (eq 1) has been studied extensively for this porpose.[3−8] Currently, the simplest and most promising system for large-scale application is powder suspension of photocatalysts. Despite exhausting efforts over 40 years, only two types of powdered catalysts such as $(Ga_{1-x}Zn_x)(N_{1-x}O_x)$[9,10] and Ru-$SrTiO_3$:Rh/$BiVO_4$[11] stably promote overall water splitting with high solar-to-chemical conversion (SCC) efficiency ≈ 0.20% under irradiation of AM1.5 simulated sunlight (1 sun). These efficiencies are higher than those of photosynthetic plants (~0.10%).[12] Recently, fabrication of photocatalyst panels based on the fixation of powdered catalysts or the epitaxial growth of semiconductor layers/arrays on specific substrates has attracted much attention because these panels absorb photons more efficiently than the powder suspension systems; some panels such as Ru-$SrTiO_3$:La,Rh/Au/$BiVO_4$[13] and GaN/InGaN[14] have succeeded in splitting water with 0.2% efficiency. Very recently, Domen et al. have reported that Cr_2O_3/Ru-$SrTiO_3$:La,Rh/Au/$BiVO_4$:Mo succeeded in splitting water with very high SCC efficiency (1.1%), although some sophisticated techniques are required for its fabrication.[15] All of these water splitting catalysts, however, face unavoidable problems: (i) the catalysts are made of rare and expensive metals (Ga, In, Au, Rh, etc.) and (ii) the generation of H_2/O_2 mixed gases hold potential explosion risks. Exploring a new artificial photosynthesis that safely produces clean solar fuels using inexpensive photocatalysts is necessary for green and sustainable energy storage.

$$H_2O \rightarrow H_2 + 1/2O_2 \quad (\Delta G^\circ = 237\ \mathrm{kJ\ mol^{-1}}) \tag{1}$$

Hydrogen peroxide (H_2O_2) is one potential solar fuel. It acts as both oxidant and reductant and can be used for electricity generation in a single-compartment direct peroxide–peroxide fuel cell (DPPFC).[16] Its theoretical potential is 1.09 V, which is comparable to that of a conventional H_2/O_2 fuel cell (1.23 V).[17] In addition, H_2O_2 is fully soluble in water and easily transportable as compared to H_2; therefore, it is a potential fuel cell energy carrier. Theoretically, H_2O_2 can be produced from earth-abundant water and O_2 by semiconductor photocatalysis. The photoformed valence band holes (VB h^+) oxidize water and produce O_2 and H^+ (eq 2). Two-electron reduction of O_2 by the conduction band electrons (CB e^-) produces H_2O_2 (eq

Received: June 7, 2016
Published: July 21, 2016

DOI: 10.1021/jacs.6b05806
J. Am. Chem. Soc. 2016, 138, 10019−10025

Scheme 1. g-C_3N_4/PDI Structures and Mechanism for Photocatalytic H_2O_2 Production[a]

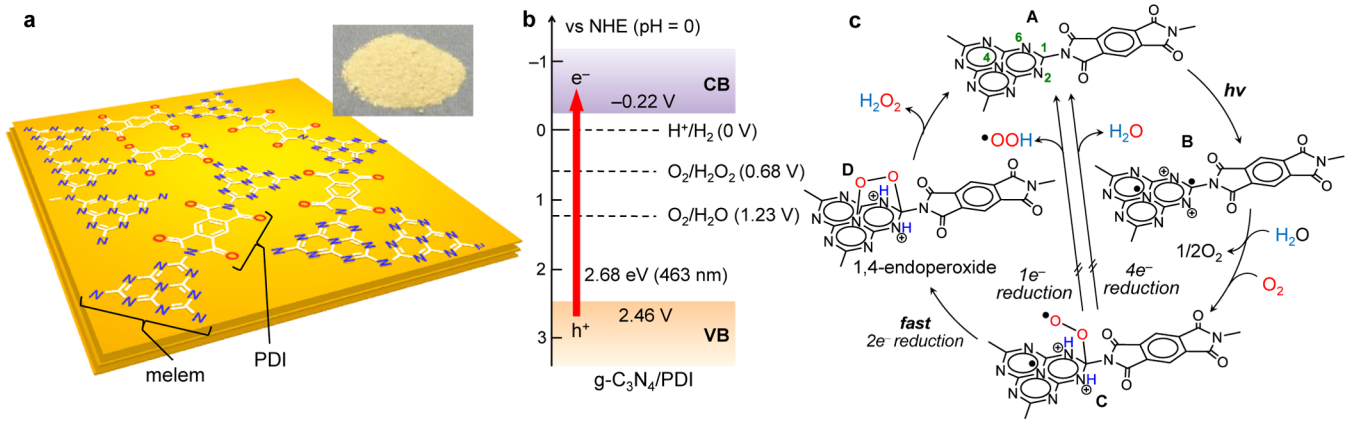

[a](a) Three-dimensional structure and (b) electronic band structure of g-C_3N_4/PDI (containing 51% PDI unit); (c) mechanism for photocatalytic H_2O_2 production.

Scheme 2. Images, Photographs, and SEM Micrographs during the Sequence for the g-C_3N_4/PDI/r$GO_{0.05}$ Synthesis

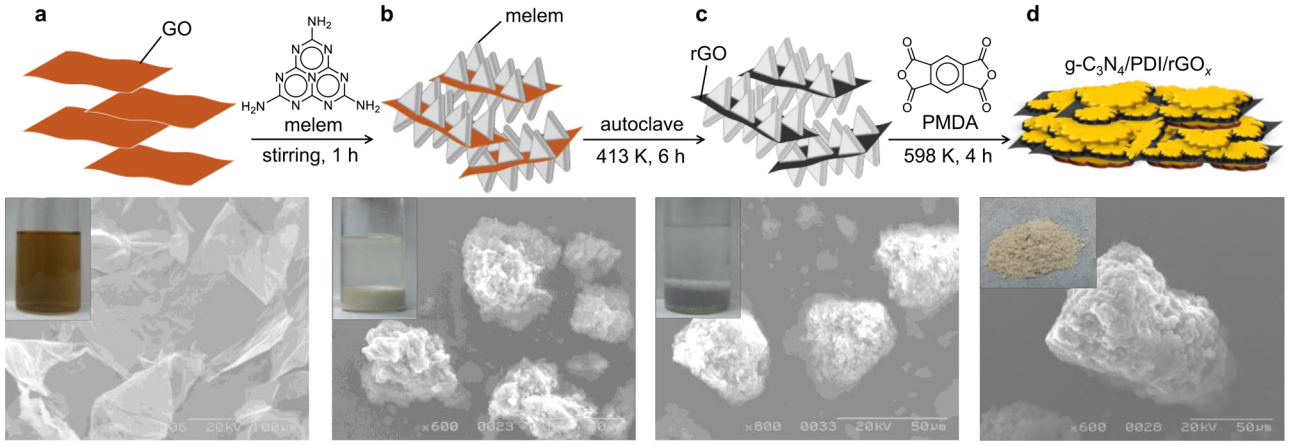

3). This facilitates solar-to-H_2O_2 energy conversion (eq 4) with relatively high free energy gain (ΔG° = 117 kJ mol^{-1}).

$$H_2O + 2h^+ \rightarrow 1/2O_2 + 2H^+ \quad (1.23\ V\ vs\ NHE) \qquad (2)$$

$$O_2 + 2H^+ + 2e^- \rightarrow H_2O_2 \quad (0.68\ V\ vs\ NHE) \qquad (3)$$

$$H_2O + 1/2O_2 \rightarrow H_2O_2 \quad (\Delta G^\circ = 117\ kJ\ mol^{-1}) \qquad (4)$$

Several inorganic-based semiconductor photocatalysts have been proposed,[18−23] but they produce only small amounts of H_2O_2 (<0.1 mM). This is because (i) they are less active for water oxidation (eq 2), (ii) they mainly promote one-electron reduction of O_2 (eq 5) or four-electron reduction of O_2 (eq 6), and (iii) they subsequently decompose the formed H_2O_2 by disproportionation or photoreaction on the surface. A new photocatalyst that efficiently promotes water oxidation and selective two-electron reduction of O_2 without decomposition of H_2O_2 is necessary.

$$O_2 + H^+ + e^- \rightarrow {}^\bullet OOH \quad (-0.13\ V\ vs\ NHE) \qquad (5)$$

$$O_2 + 4H^+ + 4e^- \rightarrow 2H_2O \quad (1.23\ V\ vs\ NHE) \qquad (6)$$

We previously found that the answer may lie in the use of organic semiconductor based on graphitic carbon nitride (g-C_3N_4).[24] We prepared g-C_3N_4 doped with pyromellitic diimide (PDI) by simple thermal condensation of melem and pyromellitic dianhydride (PMDA).[25] As shown in Scheme 1a, g-C_3N_4/PDI catalyst has a three-dimensional architecture, where the PDI units are randomly incorporated within the melem sheets and the sheets exist in layers. As shown in Scheme 1b, the catalyst has an electronic band structure capable of promoting water oxidation and two-electron reduction of O_2. As shown in Scheme 1c, photoexcitation of the catalyst at λ < 470 nm (A) leads to localization of the h^+ and e^- pairs at 2,6- and 1,4-positions on the melem unit, respectively (B). The h^+ oxidize water, and the e^- reduce O_2 creating a superoxo radical (C). Rapid reduction of the radical by another e^- at the para position creates 1,4-endoperoxide species (D), which is readily transformed to H_2O_2 by the reaction with H^+. The efficient formation of the endoperoxide species suppresses one- or four-electron reduction of O_2 (eqs 5 and 6), promoting selective two-electron reduction of O_2 (eq 3). In addition, the catalyst is inactive for decomposition of the H_2O_2 formed. This metal-free system therefore facilitates successful production of millimole per liter levels of H_2O_2. Its SCC efficiency is 0.10%, which is comparable to that of photosynthetic plants (~0.10%)[12] but lower than that of the highest levels achieved by water-splitting photocatalysts (~0.20%).[9−11] Activity improvement is therefore necessary for sunlight-driven H_2O_2 production by metal-free photocatalysts as viable artificial photosynthesis.

Here we report that simple and metal-free modification of g-C_3N_4/PDI significantly enhances the production of H_2O_2. We

DOI: 10.1021/jacs.6b05806
J. Am. Chem. Soc. 2016, 138, 10019−10025

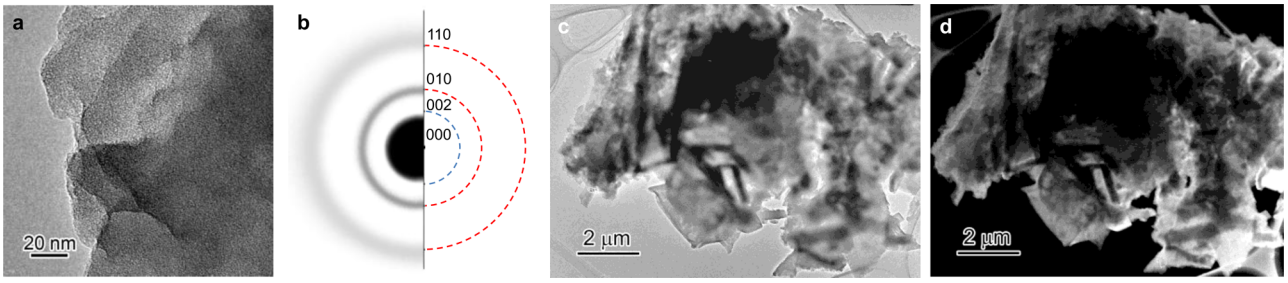

Figure 1. (a) TEM image of g-C_3N_4/PDI/$rGO_{0.05}$ and (b) its SAED pattern (inverse contrast) with indexed graphite pattern (Powder Diffraction File 56-0159, Joint Committee on Powder Diffraction Standards, [year]). (c) Bright-field and (d) dark-field TEM images of g-C_3N_4/PDI/$rGO_{0.05}$ based on the (010) diffraction.

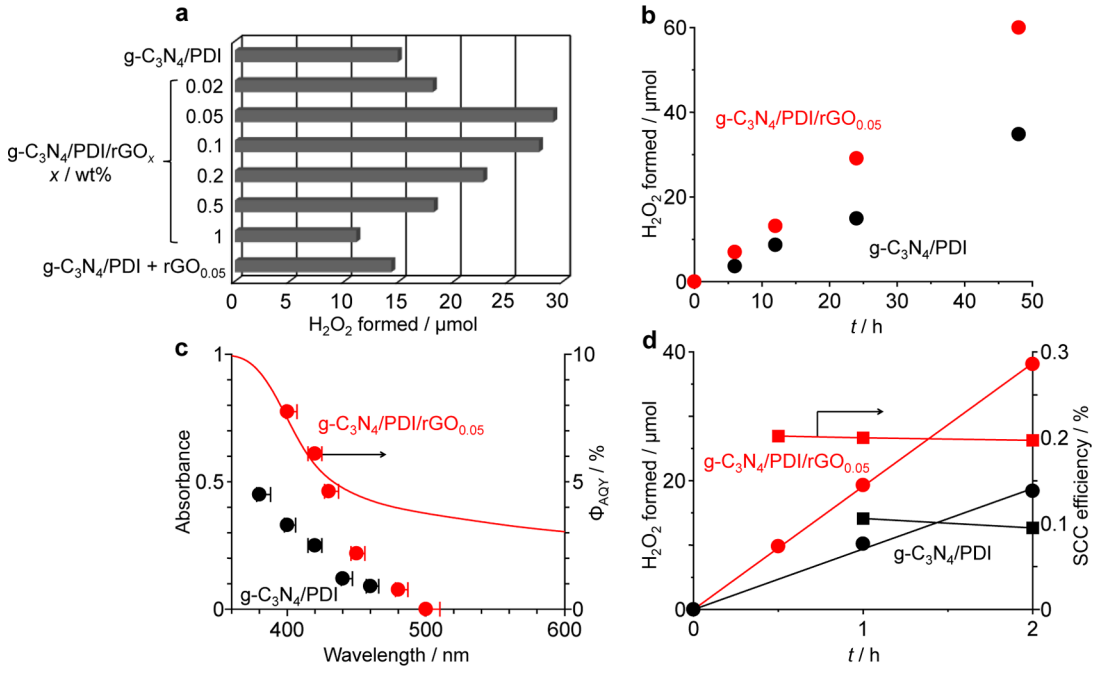

Figure 2. (a) Results for photocatalytic H_2O_2 production on the respective catalysts. Reaction conditions: water (30 mL), catalyst (50 mg), O_2 (1 atm), λ > 420 nm (Xe lamp, light intensity at 420−500 nm: 43.3 W m^{-2}), time (24 h). (b) Time-dependent change in the amounts of H_2O_2. (c) Absorption spectrum of g-C_3N_4/PDI/$rGO_{0.05}$ and action spectra for H_2O_2 formation on the respective catalysts. The apparent quantum yields for H_2O_2 formation was determined using the equation: Φ_{AQY} (%) = ([H_2O_2 formed (mol)] × 2)/[photon number entered into the reaction vessel (mol)] × 100. (d) Time-dependent change in the amounts of H_2O_2 formed and the SCC efficiencies determined under simulated AM1.5G sunlight irradiation. Reaction conditions: water (50 mL), catalyst (250 mg), O_2 (1 atm), λ > 420 nm (light intensity at 420−500 nm: 131 W m^{-2}).

used graphene, a two-dimensional single-carbon monolayer with high charge carrier mobility and high photochemical and thermal stability, which can be prepared from cheap graphite powders.[26,27] We prepared g-C_3N_4/PDI hybridized with reduced graphene oxide (rGO) by simple hydrothermal−calcination sequence. The g-C_3N_4/PDI/rGO hybrids succeeded in producing H_2O_2 with 0.20% SCC efficiency. The rGO acts as a trapping site for CB e^- of the photoexcited g-C_3N_4/PDI moiety and as an active site promoting selective two-electron reduction of O_2, thus facilitating efficient H_2O_2 production under sunlight.

RESULTS AND DISCUSSION

Catalyst Preparation. The g-C_3N_4/PDI/rGO_x hybrids were prepared by the procedure summarized in Scheme 2, where x is the amount of GO relative to the sum of the amounts of melem and PMDA [x (wt %) = GO/(melem + PMDA) × 100; melem/PMDA = 1/2(wt/wt)]. A GO solution was prepared by the Hummers' method.[28] A scanning electron microscopy (SEM) image of GO shows a flexible and wrinkled sheet[29] (Scheme 2a). Addition of white melem powders to this brown solution leads to precipitation of pale-brown powders (Scheme 2b); formation of a clear supernatant suggests that GO strongly associates with melem. SEM image of the precipitate shows ∼50 μm particles, implying that as shown by the image melem molecules are adsorbed onto GO and their aggregation creates the particles. The mixture was hydrothermally treated at 413 K for the reduction of GO (Scheme 2c).[30] Generation of gray precipitates indicates the formation of reduced GO (rGO), where the particle size (∼50 μm) scarcely changes. Calcination of the precipitates with PMDA at 598 K (Scheme 2d) gives pale-brown powders of g-C_3N_4/PDI/rGO_x with ∼100 μm diameters. The specific surface area of g-C_3N_4/PDI/$rGO_{0.05}$ (8.2 m^2 g^{-1}) is similar to that of g-C_3N_4/PDI (7.1 m^2 g^{-1}).

Characterization of Catalysts. A transmission electron microscopy (TEM) image of g-C_3N_4/PDI/$rGO_{0.05}$ shows a sheetlike structure (Figure 1a), as is the case without rGO.[25] As

DOI: 10.1021/jacs.6b05806
J. Am. Chem. Soc. 2016, 138, 10019−10025

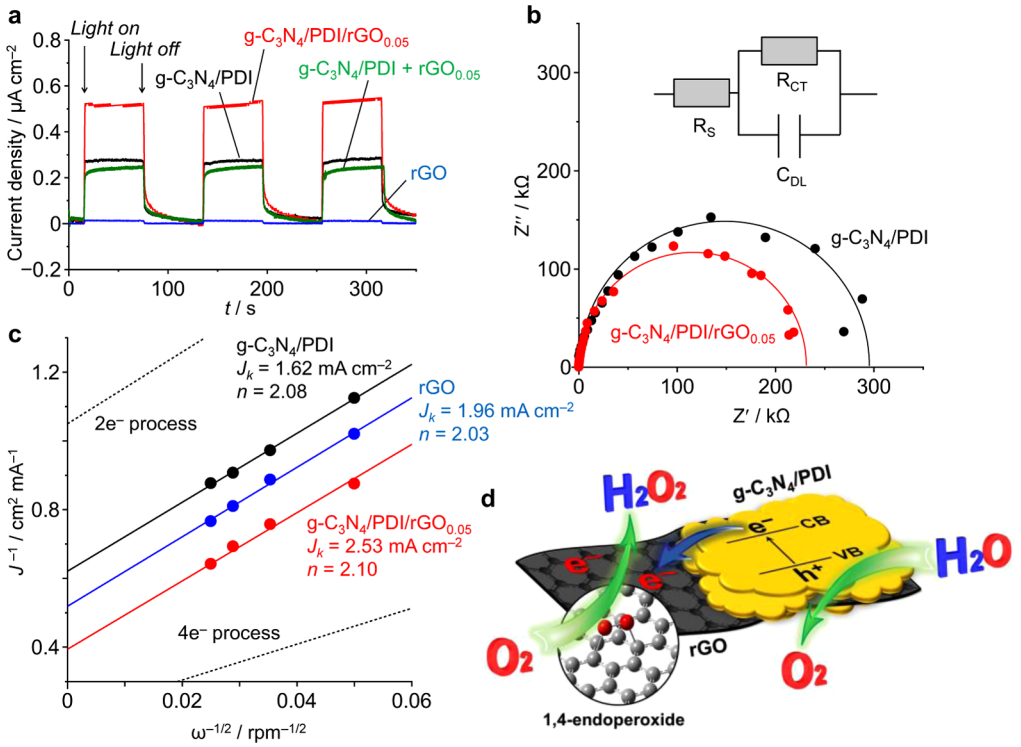

Figure 3. (a) Photocurrent response of the catalysts measured on FTO in 0.1 M Na_2SO_4 solution under visible light (λ > 420 nm) at a bias of 0.5 V (vs Ag/AgCl). (b) EIS Nyquist plots of the catalysts in 0.1 M KCl solution under visible light at a bias of 0.8 V (vs Ag/AgCl) in the frequency range of 65 mHz to 100 kHz. The electrical equivalent-circuit model (inset) was used to simulate the EIS test, where R_S is the solution resistance, C_{DL} is the constant phase element for the double layer capacitance, and R_{CT} is the charge transfer resistance across the electrode/electrolyte interface. (c) The Koutecky–Levich plots of the data obtained by RDE measurements (Figure S6) in a buffered pH 7 solution with O_2 at −0.4 V (vs Ag/AgCl). (d) Schematic illustration of the proposed mechanism for photocatalytic H_2O_2 production on g-C_3N_4/PDI/rGO.

shown in Figure 1b, its selected-area electron diffraction (SAED) pattern shows typical (110) and (010) diffractions for graphene sheets[31] but does not show (002) diffraction for graphite stacking.[32] This indicates that monolayer rGO is incorporated in the catalyst. Figure 1d shows a dark-field TEM image based on the (010) diffraction. The bright parts are distributed over the entire region, indicating that monolayer rGO is dispersed in the particles. As shown in Figure S1, powder X-ray diffraction (XRD) of g-C_3N_4/PDI/rGO$_x$ shows three peaks at 2θ = 19.0, 27.4, and 29.6 (d = 0.467, 0.325, and 0.302 nm) assigned to face-to-face stacking of PDI–PDI, melem–melem, and melem–PDI units, respectively, similar to those without rGO.[25] This suggests that the PDI units are randomly doped in the melem sheets and that the sheets are layered, as is the case without rGO (Scheme 1a), and the rGO monolayers are incorporated between the sheets (Scheme 2d). As shown in Figure S2, X-ray photoelectron spectroscopy (XPS) of g-C_3N_4/PDI/rGO$_x$ at the N 1s level shows four peaks assigned to N atoms of melem peripheral, melem center, melem amines, and imides for PDI units, as is the case without rGO.[25] Integration of these signals determined the mole fraction of the PDI units to be 50 mol % [= PDI/(melem + PDI) × 100], which is similar to that without rGO (51 mol %).[25] As shown in Figure S3, g-C_3N_4/PDI/rGO$_x$ absorbs light at λ < 470 nm, and the bandgap energies are 2.6 eV, which are also similar to those without rGO.[25]

Photoreaction. Photocatalytic reactions were performed by visible light irradiation (λ > 420 nm, Xe lamp) of pure water (30 mL) containing catalysts (50 mg) under O_2 atmosphere (1 atm) with magnetic stirring at 298 K. Figure 2a shows the amount of H_2O_2 formed by 24 h of reaction on the respective catalysts. g-C_3N_4/PDI catalyst produces 14 μmol of H_2O_2. The activity is much enhanced by hybridization of rGO; among the catalysts, g-C_3N_4/PDI/rGO$_{0.05}$ produces the largest amount of H_2O_2 (29 μmol), which is more than twice that without rGO.[33] Loading a larger amount of rGO (x > 0.05), however, decreases the activity because larger amount of rGO strongly absorbs light at λ > 400 nm[27] (Figure S3) and suppresses photoexcitation of the catalyst. It must be noted that a physical mixture of g-C_3N_4/PDI and rGO (0.05 wt %) shows almost no activity enhancement, suggesting that strong interaction of g-C_3N_4/PDI with rGO is necessary. As shown in Table S1, g-C_3N_4/PDI, when hybridized with rGO by the procedures different from those in Scheme 2, exhibits only a small activity enhancement. This suggests that the procedure in Scheme 2 leads to strong interaction between g-C_3N_4/PDI and rGO and exhibits high photocatalytic activity.

Photocatalytic Activity. Figure 2b shows the time-dependent change in the amounts of H_2O_2 formed. The rate of H_2O_2 formation on g-C_3N_4/PDI/rGO$_{0.05}$ is almost constant even after prolonged photoirradiation. This indicates that the catalyst stably produces H_2O_2 without loss of activity and scarcely decomposes the H_2O_2 formed at this concentration range,[34] as is the case without rGO.[25] It must also be noted that H_2 gas is not detected during the reactions, indicating that the system is safe from the explosion risk by H_2/O_2 mixed gases. Figure 2c shows the action spectrum for H_2O_2 formation on g-C_3N_4/PDI/rGO$_{0.05}$ determined by monochromated light irradiation. The apparent quantum yields (Φ_{AQY}) agree well with the absorption spectrum of the catalyst, indicating that its

DOI: 10.1021/jacs.6b05806
J. Am. Chem. Soc. 2016, 138, 10019–10025

bandgap excitation produces H_2O_2. Φ_{AQY} at 420 nm is determined to be 6.1%, which is more than double of that without rGO (2.6%). As shown in Figure 2d, the SCC efficiency for the H_2O_2 formation on g-C_3N_4/PDI/$rGO_{0.05}$ is determined by AM1.5G simulated sunlight (1 sun) irradiation to be 0.20% (see the Experimental Section) and is almost constant even after prolonged photoirradiation. This efficiency is comparable to the highest levels obtained by powdered water splitting photocatalysts,[9−11] suggesting that the H_2O_2 production by the metal-free photocatalyst shows potential as viable artificial photosynthesis for inexpensive, green, and sustainable solar-to-chemical energy conversion.

Half Reactions. The hybridization of g-C_3N_4/PDI with rGO enhances charge separation of the photoformed h^+ and e^- and accelerates both water oxidation (eq 2) and O_2 reduction (eq 3). The half reactions with sacrificial reagents confirm this. As shown in Figures S4 and S5, the amount of O_2 formed by water oxidation with $AgNO_3$ as a sacrificial electron acceptor and the amount of H_2O_2 formed by O_2 reduction with 2-PrOH as a sacrificial electron donor on g-C_3N_4/PDI/$rGO_{0.05}$ are about twice of those formed on g-C_3N_4/PDI. This suggests that hybridization of rGO indeed enhances photocatalytic cycles. In addition, during the O_2 reduction (Figure S5, the selectivity for the amount of H_2O_2 formed relative to the amounts of photooxidation products (acetone and CO_2)[35] on the hybrid catalyst is 90%, which is similar to that of g-C_3N_4/PDI.[25] This suggests that the hybridization of rGO enhances the separation of photoformed charge carriers, while maintaining high selectivity for two-electron reduction of O_2.

Electron Transfer to rGO. The enhanced charge separation on the hybrid photocatalyst is due to the efficient transfer of the CB e^- photoformed on g-C_3N_4/PDI to rGO. This is confirmed by photocurrent response of the catalyst loaded on a fluorine tin oxide (FTO) electrode measured under visible light irradiation. As shown in Figure 3a, the photocurrent density of the hybrid catalyst is much larger than that of g-C_3N_4/PDI, where the rGO itself shows almost no response. This indicates that the CB e^- transfer from the photoexcited g-C_3N_4/PDI to rGO indeed enhances charge separation as observed for related semiconductor/rGO systems.[27,36,37] Photoelectrochemical impedance spectroscopy (EIS) measured under visible light irradiation further confirms this. As shown in Figure 3b, both hybrid and g-C_3N_4/PDI catalysts show semicircle EIS diagrams, typical for semiconductors. The charge transfer resistance across the electrode/electrolyte interface (R_{CT}) of the hybrid catalyst is 230 kΩ, which is much smaller than that without rGO (300 kΩ). The work function of rGO is −4.42 eV versus vacuum (equivalent to −0.08 V vs NHE, pH 0)[38] and is more positive than the CB level of g-C_3N_4/PDI (−0.22 V, Scheme 1b).[25] This clearly suggests that the CB e^- transfer from the photoexcited g-C_3N_4/PDI to rGO occurs thermodynamically favorably and promotes efficient charge separation. As shown by the green line in Figure 3a, the photocurrent response of a physical mixture of g-C_3N_4/PDI and rGO is similar to that of g-C_3N_4/PDI, which agrees well with the result of photocatalytic activity (Figure 2a). These data suggest that strong interaction of g-C_3N_4/PDI and rGO promotes efficient CB e^- transfer and enhances charge separation.

Selective Two-Electron Reduction on rGO. The e^- on rGO transferred from photoexcited g-C_3N_4/PDI promote selective two-electron reduction of O_2. Rotating disk electrode (RDE) analysis confirms this. Figure S6 shows the linear-sweep voltammograms of the catalysts on RDE under O_2 atmosphere (1 atm) at different rotating speeds. The Koutecky−Levich plots of the data obtained at a constant electrode potential (−0.4 V) are summarized in Figure 3c. The slope of the plots obtained by linear regression was used to determine the average number of electrons (n) involved in overall O_2 reduction (see the Experimental Section).[39] The n value for g-C_3N_4/PDI is 2.08, indicating that as we reported earlier[25] it promotes selective two-electron reduction of O_2 (n = 2) via the formation of 1,4-endoperoxide species (Scheme 1c). The rGO itself, when loaded on RDE, exhibits n = 2.03, suggesting that rGO also promotes two-electron reduction. Some literatures reported that photoexcited anthracene[40] or carbon nanotubes[41] consisting of condensed aromatic rings reduce O_2 and produce stable 1,4-endoperoxide species. In addition, several reports revealed that the electrodes consisting of porous carbon,[42] carbon nanofiber,[43] and nanotubes[44] with condensed aromatic rings electrochemically promote two-electron reduction of O_2 and selectively produce H_2O_2. These phenomena imply that in the present case the rGO with condensed aromatic rings may also act as the site for two-electron reduction of O_2 via the formation of 1,4-endoperoxide species. As shown by the red keys in Figure 3c, the hybrid catalyst also promotes selective two-electron reduction of O_2 (n = 2.10). In that, kinetic current density (j_k) determined from the intercept of the slope is larger than that of g-C_3N_4/PDI, meaning that the hybrid catalyst enhances O_2 reduction. This is because smooth e^- transfer from g-C_3N_4/PDI to rGO increases the conductivity, as clearly supported by the EIS data (Figure 3b). These data indicate that as schematically shown in Figure 3d the rGO hybridized with g-C_3N_4/PDI behaves as an efficient cocatalyst that promotes CB e^- transfer from photoexcited g-C_3N_4/PDI and two-electron reduction of O_2 via the 1,4-endoperoxide formation. This thus facilitates efficient H_2O_2 production.

■ CONCLUSIONS

We found that g-C_3N_4/PDI/rGO hybrid photocatalyst efficiently produces H_2O_2 from water and O_2 under visible light. Hybridized rGO enhances separation of photoformed charge carriers while maintaining high selectivity for two-electron reduction of O_2. This facilitates H_2O_2 production with high SCC efficiency 0.20%, comparable to the highest levels achieved by powdered water splitting photocatalysts. This new artificial photosynthesis has several advantages over the water splitting photocatalysis: (i) no explosion risk, (ii) metal-free catalyst, and (iii) easily transportable solar fuel (H_2O_2). Recently, artificial photosynthesis by g-C_3N_4-based catalysts has attracted growing interest in overall water splitting and CO_2 reduction.[45−47] The basic concept presented here based on the creation of metal-free g-C_3N_4-based hybrid catalysts may contribute to the design of new artificial photosynthesis for renewable clean energy storage.

■ EXPERIMENTAL SECTION

Catalyst Preparation. g-C_3N_4/PDI was prepared by calcination of a powder mixture of melem[48] (2.0 g) and PMDA (4.0 g) at 598 K under N_2 flow (heating rate: 7 K min^{-1}, holding time: 4 h).[25] GO was prepared by the Hummers' method by the oxidation of graphite powders.[28,49] g-C_3N_4/PDI/rGO_x catalysts (x = 0.02, 0.05, 0.1, 0.2, 0.5, and 1) were prepared as follows: melem (0.8 g) was added to 50 mL of GO solution (9.6, 24, 48, 96, 240, and 480 mg L^{-1}), and the mixture was stirred for 1 h at room temperature. The resultant was left in a Teflon-lined autoclave at 413 K for 6 h. The resulting powders were

DOI: 10.1021/jacs.6b05806
J. Am. Chem. Soc. 2016, 138, 10019−10025

recovered by centrifugation and dried in vacuo for 12 h. The obtained powders (0.5 g) and PMDA (1.0 g) were mixed and calcined at 598 K under N_2 flow (heating rate: 7 K min^{-1}, holding time: 4 h). rGO was prepared by hydrothermal treatment of a GO solution (4 g L^{-1}, 40 mL) at 413 K for 6 h followed by drying in vacuo for 12 h.

Photoreaction. Each respective catalyst (50 mg) was added to pure water (30 mL) within a borosilicate glass bottle (φ 35 mm; capacity, 50 mL), and the bottle was sealed with a rubber septum cap. The catalyst was dispersed well by ultrasonication for 5 min, and O_2 was bubbled through the solution for 15 min. The bottle was immersed in a temperature-controlled water bath at 298 ± 0.5 K and photoirradiated at λ > 420 nm using a 2 kW Xe lamp (USHIO Inc.)[50] with magnetic stirring. The water oxidation with $AgNO_3$ as a sacrificial electron acceptor was performed with catalyst (100 mg) in a buffered La_2O_3 (30 mg) solution (30 mL, pH 8−9) with $AgNO_3$ (10 mM) under Ar atmosphere (1 atm).[24] The O_2 reduction with 2-PrOH as a sacrificial electron donor was performed with catalyst (50 mg) in a 2-PrOH/water mixture (9/1 v/v, 30 mL) under O_2 (1 atm).[35] After the reactions, the gas phase was analyzed by GC-TCD (GC-14B, Shimadzu). The catalyst was recovered by centrifugation, and the solution was analyzed by GC-FID (GC-2010, Shimadzu).[51] The amount of H_2O_2 was determined by HPLC (Prominence UFLC, Shimadzu) equipped with an electrochemical analyzer (ED723, GL Sciences Inc.).

Action Spectrum Analysis. Photocatalytic reactions were carried out in pure water (30 mL) with catalysts (50 mg). After ultrasonication and O_2 bubbling, the bottle was photoirradiated by a Xe lamp for 12 h with magnetic stirring. The incident light was monochromated by the band-pass glass filters (Asahi Techno Glass Co.),[52] where the full-width at half-maximum (fwhm) of the lights was 11−16 nm. The photon number entered into the reaction vessel was determined with a spectroradiometer (USR-40, USHIO Inc.).

Determination of SCC Efficiency. The SCC efficiency was determined by the photoreactions with a solar simulator SX-UID502XQ (USHIO Inc.). Photoreactions were performed in pure water (50 mL) with catalysts (250 mg) under O_2 (1 atm) within a borosilicate glass bottle, where λ > 420 nm cutoff filter was used to avoid subsequent decomposition of the formed H_2O_2 by absorbing UV light.[35,53] The irradiance of solar simulator was adjusted to the AM1.5 global spectrum.[54] The SCC efficiency was calculated with[11]

$$\text{SCC efficiency (\%)} = \frac{[\Delta G \text{ for } H_2O_2 \text{ generation (J mol}^{-1})][H_2O_2 \text{ formed (mol)}]}{[\text{total input energy (W)}][\text{reaction time (s)}]} \times 100 \quad (7)$$

The free energy for H_2O_2 generation is 117 kJ mol^{-1}. The overall irradiance of the AM1.5 global spectrum (300−2500 nm) is 1000 W m^{-2}, and the irradiation area is 3.14×10^{-4} m^2. The total input power over the irradiation area is therefore determined to be 0.314 W.

Electrochemical Analysis. The working electrode was prepared with a FTO glass (2 cm^2). Catalyst (50 mg) was mixed with acetone (2 mL), and the suspension was ultrasonicated for 30 min. The slurry (20 μL) was spin-coated onto the FTO glass. After drying, the glass was annealed at 598 K for 30 min under air flow for strong adhesion of the catalyst.[55] Electrochemical analysis was performed in a three-electrode cell with an electrochemical analyzer (ModuLab XM-ECS, Toyo Corp.) using 0.1 M Na_2SO_4 as an electrolyte. The pH of the solution was adjusted to 6.6 with 0.1 M NaOH, and N_2 was bubbled through the solution 10 min prior to measurements. The working electrode was immersed in the solution with a Pt wire electrode and an Ag/AgCl electrode as the counter and reference electrodes, respectively. The working electrode was photoirradiated from the back side (FTO glass/semiconductor interface) to minimize the effect of the thickness of the semiconductor layer. The exposed area under illumination was 0.25 cm^2. EIS measurements were carried out in the three-electrode cell by applying 10 mV alternative signal versus the reference electrode over the frequency range of 65 mHz to100 kHz.[56]

RDE Measurements. The measurements were performed on a computer-controlled CHI600D advanced electrochemical system with a conventional three-electrode cell. An Ag/AgCl electrode and a Pt wire electrode were used as the reference and counter electrodes, respectively. The working electrode was prepared as follows:[57] Catalyst (20 mg) was dispersed in water (5 mL) by ultrasonication. The slurry (20 μL) was put onto a Pt disk electrode and dried at room temperature. The electrode surface was coated with a Nafion solution (1 wt %, 20 μL) and dried in air. Linear-sweep voltammograms were obtained in an O_2-saturated 0.1 M phosphate-buffered solution (pH 7) with a scan rate of 10 mV s^{-1} at different rotating speeds. After each scan, O_2 was bubbled for 5 min to saturate O_2. The average number of electrons (n) involved in the overall O_2 reduction was determined by the slopes of the Koutecky−Levich plots with the following equation:[58]

$$j^{-1} = j_k^{-1} + B^{-1}\omega^{-1/2} \quad (8)$$

$$B = 0.2nF\nu^{-1/6}CD^{2/3} \quad (9)$$

j is the measured current density at a constant potential, j_k is the kinetic current density, and ω is the electrode rotating speed (rpm), respectively. F is the Faraday constant (96 485 C mol^{-1}), ν is the kinetic viscosity of water (0.01 cm^2 s^{-1}), C is the bulk concentration of O_2 in solution (1.3×10^{-6} mol cm^{-3}), and D is the diffusion coefficient of O_2 (2.7×10^{-5} cm^2 s^{-1}), respectively.[59]

Other Analysis. Diffuse-reflectance UV−vis spectra were recorded on an UV−vis spectrophotometer (V-550, JASCO Corp.) equipped with Integrated Sphere Apparatus ISV-469, using $BaSO_4$ as a reference. XRD patterns were measured on a Philips X'Pert-MPD spectrometer. XPS analysis was carried out using a JEOL JPS-9000MX spectrometer with Mg Kα radiation as the energy source. SEM observations were performed on a Hitachi S-2250 microscope. TEM observations were performed on an FEI Tecnai G2 20ST analytical electron microscope operated at 200 kV.[60]

■ ASSOCIATED CONTENT

Supporting Information

The Supporting Information is available free of charge on the ACS Publications website at DOI: 10.1021/jacs.6b05806.

XRD patterns, XPS charts, diffuse reflectance UV−vis spectra, time-dependent changes in the amounts of O_2 and H_2O_2, linear-sweep voltammograms on RDE, photocatalytic H_2O_2 decomposition, and effect of the procedure on the photocatalytic H_2O_2 production (PDF)

■ AUTHOR INFORMATION

Corresponding Author

*shiraish@cheng.es.osaka-u.ac.jp

Notes

The authors declare no competing financial interest.

■ ACKNOWLEDGMENTS

This work was supported by PRESTO from JST.

■ REFERENCES

(1) Tachibana, Y.; Vayssieres, L.; Durrant, J. R. *Nat. Photonics* **2012**, *6*, 511−518.

(2) Berardi, S.; Drouet, S.; Francas, L.; Gimbert-Surinach, C.; Guttentag, M.; Richmond, C.; Stoll, T.; Llobet, A. *Chem. Soc. Rev.* **2014**, *43*, 7501−7519.

(3) Osterloh, F. E. *Chem. Mater.* **2008**, *20*, 35−54.

(4) Kudo, A.; Miseki, Y. *Chem. Soc. Rev.* **2009**, *38*, 253−278.

(5) Maeda, K.; Domen, K. *J. Phys. Chem. Lett.* **2010**, *1*, 2655−2661.

(6) Chen, X.; Shen, S.; Guo, L.; Mao, S. S. *Chem. Rev.* **2010**, *110*, 6503−6570.

(7) Walter, M. G.; Warren, E. L.; McKone, J. R.; Boettcher, S. W.; Mi, Q.; Santori, E. A.; Lewis, N. S. *Chem. Rev.* **2010**, *110*, 6446−6473.

DOI: 10.1021/jacs.6b05806
J. Am. Chem. Soc. 2016, 138, 10019−10025

(8) Hisatomi, T.; Kubota, J.; Domen, K. *Chem. Soc. Rev.* **2014**, *43*, 7520−7535.
(9) Maeda, K.; Teramura, K.; Lu, D.; Takata, T.; Saito, N.; Inoue, Y.; Domen, K. *Nature* **2006**, *440*, 295.
(10) Kubota, J.; Domen, K. *Electrochem. Soc. Interface* **2013**, 57.
(11) Sasaki, Y.; Nemoto, H.; Saito, K.; Kudo, A. *J. Phys. Chem. C* **2009**, *113*, 17536−17542.
(12) Reijnders, L.; Huijbregts, M. *Biofuels for Road Transport: A Seed to Wheel Perspective*; Springer Science & Business Media: New York, 2008; pp 49−57.
(13) Wang, Q.; Li, Y.; Hisatomi, T.; Nakabayashi, M.; Shibata, N.; Kubota, J.; Domen, K. *J. Catal.* **2015**, *328*, 308−315.
(14) Kibria, M. G.; Chowdhury, F. A.; Zhao, S.; AlOtaibi, B.; Trudeau, M. L.; Guo, H.; Mi, Z. *Nat. Commun.* **2015**, *6*, 6797.
(15) Wang, Q.; Hisatomi, T.; Jia, Q.; Tokudome, H.; Zhong, M.; Wang, C.; Pan, Z.; Takata, T.; Nakabayashi, M.; Shibata, N.; Li, Y.; Sharp, I. D.; Kudo, A.; Yamada, T.; Domen, K. *Nat. Mater.* **2016**, *15*, 611−615.
(16) Mousavi Shaegh, S. A.; Nguyen, N.-T.; Mousavi Ehteshami, S. M.; Chan, S. H. *Energy Environ. Sci.* **2012**, *5*, 8225−8228.
(17) Yamada, Y.; Yoneda, M.; Fukuzumi, S. *Energy Environ. Sci.* **2015**, *8*, 1698−1701.
(18) Teranishi, M.; Naya, S.; Tada, H. *J. Am. Chem. Soc.* **2010**, *132*, 7850−7851.
(19) Tsukamoto, D.; Shiro, A.; Shiraishi, Y.; Sugano, Y.; Ichikawa, S.; Tanaka, S.; Hirai, T. *ACS Catal.* **2012**, *2*, 599−603.
(20) Shiraishi, Y.; Kanazawa, S.; Tsukamoto, D.; Shiro, A.; Sugano, Y.; Hirai, T. *ACS Catal.* **2013**, *3*, 2222−2227.
(21) Kaynan, N.; Berke, B. A.; Hazut, O.; Yerushalmi, R. *J. Mater. Chem. A* **2014**, *2*, 13822−13826.
(22) Moon, G.-H.; Kim, W.; Bokare, A. D.; Sung, N.-E.; Choi, W. *Energy Environ. Sci.* **2014**, *7*, 4023−4028.
(23) Kim, H.-I.; Kwon, O. S.; Kim, S.; Choi, W.; Kim, J.-H. *Energy Environ. Sci.* **2016**, *9*, 1063−1073.
(24) Wang, X.; Maeda, K.; Thomas, A.; Takanabe, K.; Xin, G.; Carlsson, J. M.; Domen, K.; Antonietti, M. *Nat. Mater.* **2009**, *8*, 76−80.
(25) Shiraishi, Y.; Kanazawa, S.; Kofuji, Y.; Sakamoto, H.; Ichikawa, S.; Tanaka, S.; Hirai, T. *Angew. Chem., Int. Ed.* **2014**, *53*, 13454−13459.
(26) Geim, A. K.; Novoselov, K. S. *Nat. Mater.* **2007**, *6*, 183−191.
(27) Xiang, Q.; Yu, J.; Jaroniec, M. *J. Phys. Chem. C* **2011**, *115*, 7355−7363.
(28) Hummers, W. S.; Offeman, R. E. *J. Am. Chem. Soc.* **1958**, *80*, 1339.
(29) Zhu, B. Y.; Murali, S.; Cai, W.; Li, X.; Suk, J. W.; Potts, J. R.; Ruoff, R. S. *Adv. Mater.* **2010**, *22*, 3906−3924.
(30) Zhou, Y.; Bao, Q.; Tang, L. A. L.; Zhong, Y.; Loh, K. P. *Chem. Mater.* **2009**, *21*, 2950−2956.
(31) Zhang, J.; Yang, H.; Shen, G.; Cheng, P.; Zhang, J.; Guo, S. *Chem. Commun.* **2010**, *46*, 1112−1114.
(32) Choucair, M.; Thordarson, P.; Stride, J. A. *Nat. Nanotechnol.* **2009**, *4*, 30−33.
(33) The g-C_3N_4/PDI/r$GO_{0.05}$ catalysts were prepared three times under the same conditions and used for photoreactions. They show almost the same activity for H_2O_2 production with the deviation of ±3%, indicative of sufficient reproducibility of the catalysts.
(34) The formed H_2O_2 is further oxidized (decomposed) by h^+ at high concentration. As shown in Figure S7, a H_2O_2 (ca. 100 μmol) solution, when stirred with the catalyst in the dark (green), is scarcely decomposed. Photoirradiation of this solution with O_2 increases the H_2O_2 amount, but the increasing rate is slower than that in pure water. This suggests that oxidation of H_2O_2 by h^+ scarcely occurs at low H_2O_2 concentration but occurs more easily at higher H_2O_2 concentration. Almost linear H_2O_2 formation (Figure 2b) is because of the low H_2O_2 concentration.
(35) Shiraishi, Y.; Kanazawa, S.; Sugano, Y.; Tsukamoto, D.; Sakamoto, H.; Ichikawa, S.; Hirai, T. *ACS Catal.* **2014**, *4*, 774−780.
(36) Jia, L.; Wang, D.-H.; Huang, Y.-X.; Xu, A.-W.; Yu, H.-Q. *J. Phys. Chem. C* **2011**, *115*, 11466−11473.
(37) Yang, M.-Q.; Weng, B.; Xu, Y.-J. *Langmuir* **2013**, *29*, 10549−10558.
(38) Gao, E.; Wang, W.; Shang, M.; Xu, J. *Phys. Chem. Chem. Phys.* **2011**, *13*, 2887−2893.
(39) Sheng, H.; Ji, H.; Ma, W.; Chen, C.; Zhao, J. *Angew. Chem., Int. Ed.* **2013**, *52*, 9686−9690.
(40) Fidder, H.; Lauer, A.; Freyer, W.; Koeppe, B.; Heyne, K. *J. Phys. Chem. A* **2009**, *113*, 6289−6296.
(41) Dukovic, G.; White, B. E.; Zhou, Z.; Wang, F.; Jockusch, S.; Steigerwald, M. L.; Heinz, T. F.; Friesner, R. A.; Turro, N. J.; Brus, L. E. *J. Am. Chem. Soc.* **2004**, *126*, 15269−15276.
(42) Liu, Y.; Quan, X.; Fan, X.; Wang, H.; Chen, S. *Angew. Chem., Int. Ed.* **2015**, *54*, 6837−6841.
(43) Yamanaka, I.; Murayama, T. *Angew. Chem., Int. Ed.* **2008**, *47*, 1900−1902.
(44) Gao, G.; Zhang, Q.; Hao, Z.; Vecitis, C. D. *Environ. Sci. Technol.* **2015**, *49*, 2375−2383.
(45) Zhang, G.; Lan, Z.-A.; Lin, L.; Lin, S.; Wang, X. *Chem. Sci.* **2016**, *7*, 3062−3066.
(46) Niu, P.; Yang, Y.; Yu, J. C.; Liu, G.; Cheng, H.-M. *Chem. Commun.* **2014**, *50*, 10837−10840.
(47) He, Y.; Zhang, L.; Teng, B.; Fan, M. *Environ. Sci. Technol.* **2015**, *49*, 649−656.
(48) Chu, S.; Wang, C.; Feng, J.; Wang, Y.; Zou, Z. *Int. J. Hydrogen Energy* **2014**, *39*, 13519−13526.
(49) Chen, J.; Yao, B.; Li, C.; Shi, G. *Carbon* **2013**, *64*, 225−229.
(50) Sugano, Y.; Shiraishi, Y.; Tsukamoto, D.; Ichikawa, S.; Tanaka, S.; Hirai, T. *Angew. Chem., Int. Ed.* **2013**, *52*, 5295−5299.
(51) Sakamoto, H.; Ohara, T.; Yasumoto, N.; Shiraishi, Y.; Ichikawa, S.; Tanaka, S.; Hirai, T. *J. Am. Chem. Soc.* **2015**, *137*, 9324−9332.
(52) Shiraishi, Y.; Sakamoto, H.; Sugano, Y.; Ichikawa, S.; Hirai, T. *ACS Nano* **2013**, *7*, 9287−9297.
(53) Goldstein, S.; Aschengrau, D.; Diamant, Y.; Rabani, J. *Environ. Sci. Technol.* **2007**, *41*, 7486−7490.
(54) American society for testing and materials (ASTM). Reference Solar Spectral Irradiance: Air Mass 1.5. http://rredc.nrel.gov/solar/spectra/am1.5 (accessed March 2016).
(55) Zhang, J.; Sun, J.; Maeda, K.; Domen, K.; Liu, P.; Antonietti, M.; Fu, X.; Wang, X. *Energy Environ. Sci.* **2011**, *4*, 675−678.
(56) Hu, S.; Ma, L.; Wang, H.; Zhang, L.; Zhao, Y.; Wu, G. *RSC Adv.* **2015**, *5*, 31947−31953.
(57) Zheng, Y.; Jiao, Y.; Chen, J.; Liu, J.; Liang, J.; Du, A.; Zhang, W.; Zhu, Z.; Smith, S. C.; Jaroniec, M.; Lu, C. Q.; Qiao, S. Z. *J. Am. Chem. Soc.* **2011**, *133*, 20116−20119.
(58) Lin, L.; Zhu, Q.; Xu, A. *J. Am. Chem. Soc.* **2014**, *136*, 11027−11033.
(59) Liu, Y.; Liu, H.; Wang, C.; Hou, S.-X.; Yang, N. *Environ. Sci. Technol.* **2013**, *47*, 13889−13895.
(60) Shiraishi, Y.; Tanaka, K.; Shirakawa, E.; Sugano, Y.; Ichikawa, S.; Tanaka, S.; Hirai, T. *Angew. Chem., Int. Ed.* **2013**, *52*, 8304−8308.

DOI: 10.1021/jacs.6b05806
J. Am. Chem. Soc. 2016, 138, 10019−10025